International Journal of Engineering and Technical Research (IJETR)
ISSN: 2321-0869 (O) 2454-4698 (P) Volume-8, Issue-2, February 2018

Digital Image Processing System to determine Sea Ice Parameters based on Field Observation on Offshore Platform

Huihui Li, Jiwen Song

***Abstract*— Sea ice has negative influence on oil/gas platforms, nautical transportation and offshore operations during the ice-covered season of the Bohai Sea. The accurate, continuous and real-time field observations of sea ice parameters are important for reliability analysis of oil and gas exploration, validation of sea ice numerical models and revision of satellite remote sensing data. We adopted modern digital image techniques, and developed an efficient software system to collect, process and obtain ice thickness, ice concentration and ice velocity, respectively. With the application to the JZ20-2 oil/gas field of the Liaodong Bay during the winter of 2009-2010, preliminary results of ice thickness, concentration and velocity were obtained. It shows that the sea ice digital image acquisition and processing system has the advantages of convenient operation, high accuracy and reliability. With further improvements, it can be extended and applied in the sea ice field observations of the Baohai Sea.**

***Index Terms*— ice thickness, ice concentration, ice velocity, filed observation, digital image techniques.**

I. INTRODUCTION

Field monitoring of sea ice parameters are of primary importance for sea ice forecasting, and the development of accurate sea ice thermo-dynamic numerical model. Ice thickness, ice concentration and ice velocity are the three most important ones. Measurement techniques for ice thickness include ship based radar, upward looking sonar, electromagnetic induction, satellite imagery and digital image techniques, besides visual measurement (Drucker and Martin, 2003; Haas, 1998; Haas et al., 2009; Niioka and CHO, 2010; Toyota et al., 2009; Worby et al., 1999). Ice concentration data have been obtained mainly by visual measurement with strong subjectivity. Synthetic aperture radar has been used to determine ice concentration. However, it has limited spatial coverage. Passive microwave satellite remote sensing, with its wide synoptic view and relatively high precision, has been used to extract the ice concentration information in the polar region, and generally provides good results compared with synthetic aperture radar (Knuth and Ackley, 2006; Worby and Comiso, 2004). Satellite remote sensing measurements, however, are easily affected by climate and receiving interval, and cannot get continuous data, compared with synthetic aperture radar. Sea ice velocities are normally monitored with marine radar, buoys and satellite remote sensing (Heil et al. 2001; Vesecky et al., 1988). Buoys have the disadvantage of high cost or weak continuity.

Due to these limitations in ice field observation, new monitoring techniques are needed to obtain ice parameters continuously and precisely in the oil/gas fields. Modern digital image analysis techniques have been preliminarily applied in the ice concentration monitoring in the ice breaker investigation in the polar region, because of its high precision, low cost and easy operation (Hall et al., 2002; Lu et al., 2010; Muramoto et al., 1993; Weissling et al., 2009).

In China, field observations of sea ice parameters started in early 1960s, and different techniques have been developed since then. Sea ice in the Bohai Sea, compared with fast ice in the polar region, has the characteristics of high flowability and low thickness. It is not suitable to perform contact measurement on the ice surface to get ice thickness. Ice concentration data were obtained by human visual measurements, and the results unavoidably depend on the experience of observers, and are also affected by visibility. Relatively ideal velocities have been obtained by using marine radar. This method, however, involves manpower, and can not get velocities continuously during the whole ice period.

Therefore, the objective of this study is to realize fixed point monitoring of sea ice parameters based on offshore platforms using digital image acquisition and processing technique. Videos and digital images are continuously collected and processed, and ice thickness, concentration and velocity are obtained through a digital image processing software system developed using OpenCV and C# language. We applied the system on the JZ20-2 oil/gas field in the Liaodong Bay during the winter of 2009-2010, and monitored continuously the sea ice parameters of the whole ice period. The obtained sea ice data provide timely and reliable reference for early warning and protection for ice damage.

II. DIGITAL IMAGE TECHNIQUE FOR SEA ICE PARAMETERS

A. Digital image technique for sea ice thickness

When sea ice interacts with the conical structure on the pile of the platform, flexural failure may happen, and the ice thickness cross section is clearly displayed with the overturn of the ice after its breakage. The marginal points of sea ice are extracted after corrections to the collected images of the ice breakup process, and the corresponding pixel points of the ice thickness are predicted. The length of the pixel points are then calibrated by a characteristic length of the conical structure.

Fig.1 shows the schematic of ice thickness measurement. A characteristic length AB, here the diameter of the cone, is chosen and calibrated, and the thickness ti, is measured after ice break-up. The real thickness of sea ice can be calculated based on the proportional relationship between the diameter of the cone and the ice thickness,

Huihui Li, Beijing Branch, CNOOC Information Technology CO, Ltd, Beijing, China.
Jiwen Song, Beijing Branch, CNOOC Information Technology CO, Ltd, Beijing, China.

$$t_i = D\frac{r_i}{r_D} \tag{1}$$

where D is the diameter of the cone, ri is the pixel length of ice thickness and rD is the pixel length of the cone diameter. Usually, three different ice thicknesses are chosen to reduce the measurement error. For example, the thicknesses are 13.2cm, 13.7cm and 13.9cm, respectively, of the three different cross sections of the sea ice shown in Fig. 1.

In fact, the ice thickness measurement is the measurement of distance, and has the advantage of high stability and strong operability. The measurement error is attributed to the image resolution and analytical technique. However, the sunlight, climate and measurement angle in the field observation will also produce some measurement error. In order to improve the reliability of the monitored data, the observation was performed perpendicularly to the conical structure and the ice thickness cross section. This was considered when installing CCD, and statistic analysis was carried out to multiple sets of measurement data.

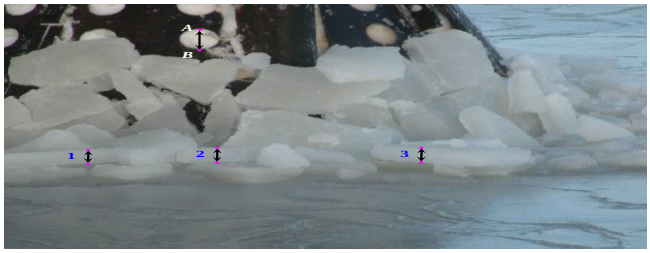

Fig.1 The schematic of ice thickness measurement.

B. Digital image technique for sea ice concentration

The process of the determination of sea ice concentration includes image correction and parameter identification. Image distortion exists to some extent due to the shooting angle when shooting or videoing from the platform, and needs to be corrected. Image recognition is mainly to determine the proportion of sea water and sea ice through image segmentation.

We used the maximum between-class variance (Otsu method) to segment sea water and sea ice (Otsu, 1979). The key point is to identify and extract the object (sea ice) from the background (sea water). Global threshold segmentation algorithm is usually used to segment the image. The image is first enhanced with Homo-morphic filtering method, then inpainted with morphological method after image edge detection, and the binary image is obtained. By multiplying the image correction matrix, the proportion of the white pixels in all the pixels is calculated and the ice concentration is obtained.

The simple global threshold segmentation algorithm, however, cannot meet the precision requirement when the demarcation line is not so clear between ice and water due to the effect of sunlight, shadow and climate. Thus, the adaptive threshold segmentation algorithm was adopted with the following three improvements: 1) Compress the image to reduce the computational complexity; 2) Enhance the image contrast by equalizing the grey scale; 3) Evaluate the optimum threshold value to simplify the segmentation algorithm.

Assume the threshold value t segments the grey scale with L levels into two classes: $C_0 \in [0,t]$ and $C_1 \in [t+1, L-1]$. After the normalization of the image histogram, the pixel distribution probability of grey scale i can be calculated as (Otsu, 1979),

$$P_i = \frac{n_i}{N}\left(P_i \geq 0, \sum_{i=0}^{L-1} P_i = 1\right) \tag{2}$$

where N is the total pixels, n_i is the pixel of grey scale i. The occurrence probability and average value of C_0 and $C_1$are (Otsu, 1979),

$$w_0 = p_r(C_0) = \sum_{i=0}^{t} p_i = w(t) \tag{3}$$

$$w_1 = p_r(C_1) = \sum_{i=t+1}^{L-1} p_i = 1 - w(t) \tag{4}$$

Based on Otsu method, the between-class variance of C_0 and C_1 is (Otsu, 1979),

$$\begin{aligned}\sigma_B^2 &= w_0(u_0 - u_T)^2 + w_1(u_1 + u_T)^2 \\ &= w_0 w_1 (u_1 - u_0)^2\end{aligned} \tag{5}$$

With $u_T = \sum_{i=0}^{L-1} ip_i$, $u_0 = \sum_{i=0}^{t} \frac{ip_i}{w_0} = \frac{u(t)}{w(t)}$, $u_1 = \sum_{i=t+1}^{L-1} \frac{ip_i}{w_1} = \frac{u_T - u(t)}{1 - w(t)}$.

Thus, the optimal threshold value $t^* = \arg\max_{0 \leq t \leq L-1} \sigma_B^2$ is to make the maximum between-class variance.

The image processing method has the advantages of simple calculation and high stability. It is suitable for over 90% of all images, and can be programmed to realize batch image processing. For example, Fig.2 is the collected image and its binary image of the segmentation of ice and water at 13:30 on Jan. 1, 2010 on the JZ20-2 sea area, and the ice concentration is 86.1%. In addition, considering the interference of the sea level in the digital image (as in Fig.3), a function to extract the sea level is added in the concentration identification. With the definition of the sea horizon, the sky on the upper image is deleted and only the image under the sea horizon is processed. In this way, the problem of mistaking the sky as sea ice is effectively solved. The sea ice concentration identification results reflect the real condition of sea ice objectively.

Concerning the sea ice concentration extraction during the digital image processing, the resolution, the choice of threshold value and computational precision will unavoidably induce measurement error. The position and gesture of the video camera is another main factor inducing measurement error. Only when the CCD of the video camera is perpendicular to the measured surface, the error induced by image distortion can be reduced to the minimum. However, shooting angle exists to some extent when shooting the sea ice far from the observation point. Reasonable planar rectification is an important issue in the digital image recognition.

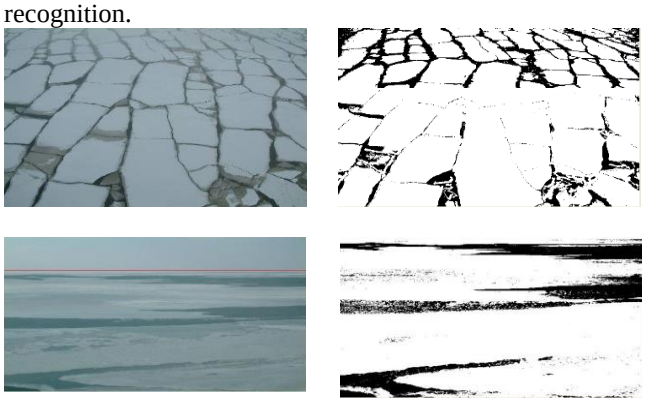

Fig. 3 Ice image and its binary image with the function of sea level extraction.

C. Digital image technique for sea ice velocity

The calculation of speed and direction of sea ice velocity can be realized through the extraction and matching of feature points at different times. Multiple image sequences of the same time interval are extracted, and the ice speed is determined by the comparison of feature points of neighboring sequences. Feature points are the pixel points on the border of different heights in the image, and the corner feature is considered to reduce the computational complexity and increase the matching speed. The Harris corner detection algorithm was used here to extract feature points (Harris and Stephens, 1988).

The Harris corner is extracted from a grey scale. It is the point with an acute change of the grey scale, and can be determined by the calculation of the gradient and curvature of the corner. If the coordinates of the two dimensional pixel point are (x, y), the Harris corner point is expressed as (Harris and Stephens, 1988),

$$E(x,y)=\sum_{u,v} w(u,v)[I(x+u,y+v)-I(u,v)]^2 =[u,v]M\begin{bmatrix}u\\v\end{bmatrix} \quad (6)$$

$$M=\sum_{u,v} w(u,v)\begin{bmatrix}I_x{}^2 & I_xI_y\\ I_xI_y & I_y{}^2\end{bmatrix} \quad (7)$$

where I is the image pixel matrix, w is the smooth function of noise reduction, I_x, I_y and I_x^2, I_y^2 are the first and second order partial differential of the pixel in the horizontal and vertical direction, respectively, (u, v) are the offset coordinates. Thus, the corner points of the image can be detected through the following equation (Harris and Stephens, 1988),

$$R=\det(M)-k\,tr(M)^2 \qquad k\in[0,0.04] \quad (8)$$

With the determination of feature points through the Harris operator, the displacement of sea ice can be obtained by matching corresponding feature points in different images. Here we adopted a simple guided complementary matching algorithm to match feature points. When feature points are not obvious, mismatches will be produced and induce computational error. The mismatches are eliminated with the application of a clustering method based on greedy EM algorithm for Gaussian mixture learning (Vlassis and Likas, 2002). The Gaussian mixture model can be described as (Vlassis and Likas, 2002),

$$f_k(x)=\sum_{j=1}^{k} w_j\phi(x;\theta_j) \quad (9)$$

With

$$\phi(x;\theta_j)=\phi(x;m_j,\sigma_j)=(2\pi)^{-\frac{d}{2}}\left|\sigma_j\right|^{-\frac{1}{2}\exp(-\frac{1}{2}(x-m_j)^T\sigma_j^{-1}(x-m_j))} \quad (10)$$

here $\phi(x;\theta)$ is the j^{th} component and a d-dimensional Gaussian density with θ_j as a parameter. w_j is the mixture coefficient of the j^{th} component. k is the number of components. m_j and σ_j are the average value and covariance matrix of the j^{th} component.

With the Harris operator, the feature point extraction is reasonable and uniform, and can be extracted quantitatively according to the real circumstances. In addition, it maintains robustness when images are under such conditions as rotation, change of grey scale, noise influence and change of viewing angle (Cordelia et al., 2000). Fig. 4 shows the feature points and their movements at different times monitored starting at 09:20 on Feb 15, 2010, and ice velocities are determined as (76.79cm/s, 278.19°), (77.96cm/s, 278.86°) and (79.26cm/s, 279.11°), and the average value is (78.00cm/s, 278.72°). Here the upward direction is defined as 0°, and clockwise downward is defined as 180°. The angles in the collected images need to be georeferenced to determine the ice direction in geographic coordinates in field observations.

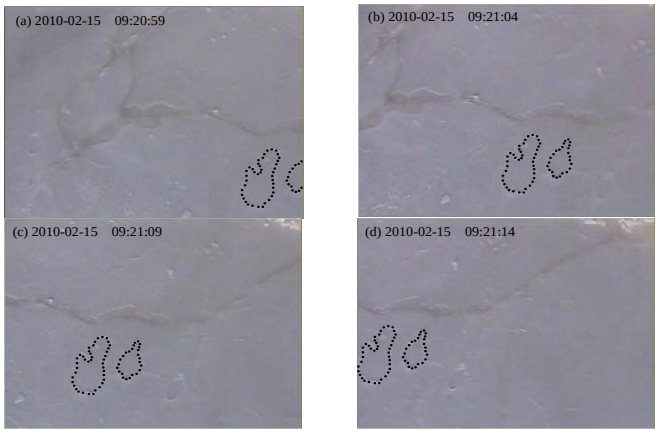

Fig.4 Sketch of the extraction of feature points in the monitoring of sea ice velocity.

The measurement errors of ice velocities are from the precision of the ice velocity calibration parameters and the computational precision of the extraction and matching of the feature points. In addition, the platform will vibrate under ice loads, and this will produce an instability of the marking of corner points. Thus, to reduce the measurement error, it is necessary to determine precisely the calibration parameters and perform statistical analysis on multiple sets of measurement data of ice velocities.

III. DIGITAL IMAGE PROCESSING SOFTWARE FOR OBTAINING SEA ICE PARAMETERS

We developed a sea ice digital image acquisition and processing system using OpenCV and C# language. It consists of three modules of ice thickness, ice concentration and ice velocity with the transferability between modules, and has the function of simultaneous storage of multiple sets of measurement results. For each module, the collected digital images or video are first imported to the corresponding measurement interface. For videos, the playing speed can be set and the specified interface can be saved as image format.

In the ice thickness measurement module, through the setting and calibration function of the reference on the interface, the corresponding physical length of every pixel can be obtained. In addition, in order to enhance the resolution at the edge, this module has enlargement function to precisely determine the needed references and pixels at the edge. In the ice concentration measurement module, after pre-processing on the image edges, binary images are created with image correction. The Otsu method is then used to segment sea water and sea ice in the binary image, and the proportion of sea ice in the total area, i.e., the concentration, is determined. In the ice velocity measurement module, continuous measurements of ice velocity at different times can be determined by the extraction of feature points in the video image, the matching of feature points in different image sequences, and the elimination of the mismatching points. The calibration function is integrated in the velocity module and used to

determine the corresponding physical length of the pixels and the corresponding angles between the image and geographic orientation. The real-time computing function performs real-time computation on the current display of the video and gives the corresponding real ice speed and direction. Moreover, a quick browsing function is also added in the module and the needed clips can be quickly selected from the video. The system has the characteristics of precise calculation, easy operation and friendly interface.

IV. Applications in the Bohai Sea Ice

The Bohai Sea JZ20-2 oil/gas field (north latitude 40°31′, east longitude 121°21′) is located at north Liaodong Bay as shown in Fig.5. The sea freezes in winters. Field observations have been carried out mainly on the JZ20-2 platform each winter since its operation in 1990s. The JZ20-2 platform consists of a central platform (that is, Zhongbei platform), unattended Beigaodian and Zhongnan platform, Nan and 211 satellite platform, and the central platform is composed of MUQ, MNW and BOP platform connected through piers as shown in Fig. 6. A comprehensive sea ice field observation system has been established on JZ20-2 platform, and remote control and data transfer between monitoring instruments on other platforms are realized through wireless network. Field measurements on JZ20-2 oil/gas field consist of three parts: (1) Ice parameters measurements including ice thickness, ice concentration, ice velocity, ice amount and ice type. (2) Meteorological factors such as wind velocity, temperature, relative humidity and atmospheric pressure. (3) Iced induced vibration of the platform structure and upper oil and gas pipelines. During the winder of 2009-2010, we used the digital image acquisition and processing system to obtain ice thickness, ice concentration and ice velocity on the JZ20-2 sea area.

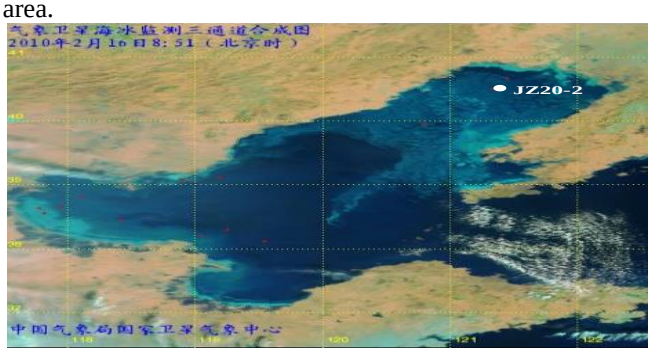

Fig. 5 The location of the JZ20-2 oil/gas field

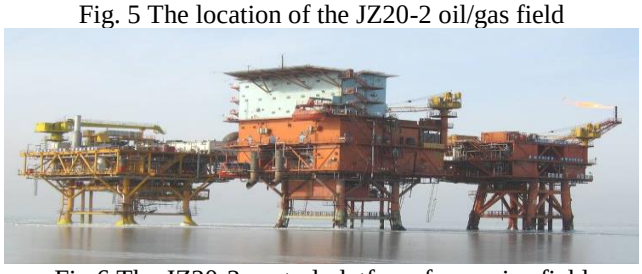

Fig.6 The JZ20-2 central platform for sea ice field observation of the Liaodong Bay

Ice thickness and velocity were collected by the two CCDs installed at different positions on the middle layer of the deck. The CCD used to measure thickness is perpendicular to the upper surface of the conical structure on the platform pile to collect the cross section data after ice breakage. The CCD used to measure ice velocity is perpendicular to the ice surface to collect video as the ice drifts. The two CCDs switch automatically every 30 seconds, and a set of 2-min images were collected every 20 minutes. The ice concentration images were collected by the digital camera installed at the upper deck, shooting every hour during the day.

Fig.7 and Fig.8 show the ice thickness and ice concentration obtained by the digital image techniques during the winter of 2009-2010 on the JZ20-2 platform, in which all values are daily average values. Fig.9 plots the ice velocity vector measured continuously between 00:00 Feb 2, 2010 and 00:00 Feb 6, 2010. The tidal component calculated through 2-D shallow water wave equation is also included in Fig.9. It shows that the ice flow is controlled by the tide during this period. In addition, the speeds in the x direction at the 60th and 94th hour are obviously higher due to the effect of wind drag.

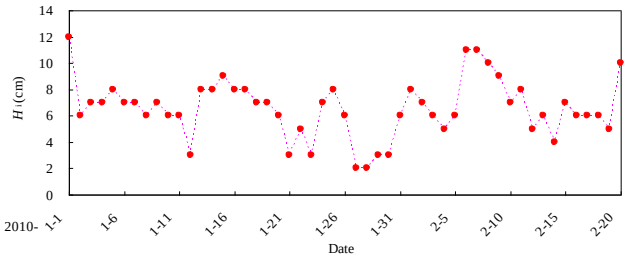

Fig.7 The daily average ice thickness of the winter of 2009-2010 on the JZ20-2 sea area.

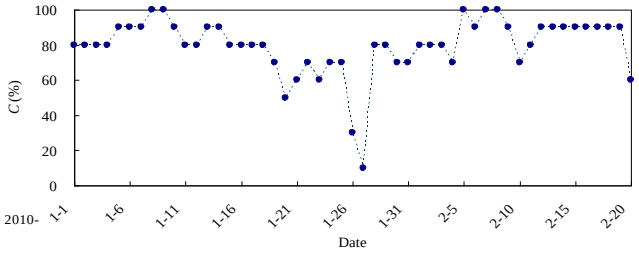

Fig.8 The daily average ice concentration of the winter of 2009-2010 on the JZ20-2 sea area.

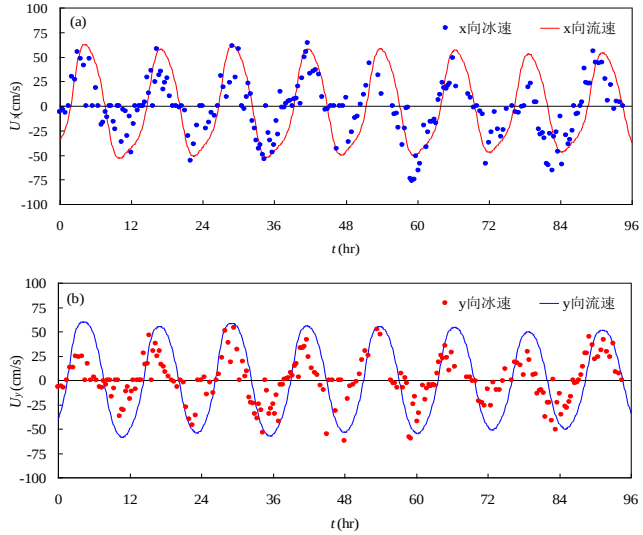

Fig.9 Measured and calculated ice velocity (From 00:00 Feb 2, 2010 to 00:00 Feb 6, 2010).

V. Conclusions

With respect to sea ice management of the Liaodong Bay oil/gas field, much attention has been paid to the precision, continuity and completeness of the field monitoring of sea ice parameters. We developed a data acquisition and processing

system for field monitoring of ice thickness, concentration and velocity using digital image technique considering its advantages of easy operation, low cost and high precision. We developed a software system with high precision and a user-friendly interface using OpenCV and C# language. We used the system on the JZ20-2 platform and obtained detailed ice data of the 2009-2010 winter.

To better apply the developed sea ice digital image acquisition and processing system in oil/gas exploitation areas, it is necessary to make following improvements in the next work: 1) Adopt infrared ray image monitoring technique to collect continuously and extract ice parameters 24 hours a day. 2) Realize the real-time field monitoring and data extraction. 3) Apply the system further to other oil/gas platforms, and form fixed point field observation network and get complete ice information in the Liaodong Bay. With above improvements, the developed digital image system can be extended and applied to the field observation of oil/gas fields in the Bohai Sea, and provide reliable technical support for ice management.

ACKNOWLEDGMENT

The authors appreciate the support of the staff on the JZ20-2 platform for their assistance during the field observation. This study was support by the CNOOC project with grant No. RD0102C05.

REFERENCES

[1] Drucker, R. and Martin, S., 2003, Observations of ice thickness and frazil ice in the St. Lawrence Island polynya from satellite imagery, upward looking sonar, and salinity/temperature moorings, Journal of Geophysical Research, 108(C5): 3149, doi:10.1029/2001JC001213.

[2] Haas, C., 1998. Evaluation of ship-based electromagnetic-inductive thickness measurements of summer sea-ice in the Bellingshausen and Amundsen Seas Antarctica. Cold Regions Science and Technology, 27, 1-16.

[3] Haas, Christian, Lobach, John, Hendricks, Stefan, Rabenstein, Lasse, Pfaffling Andreas, 2009. Helicopter-borne measurement of sea ice thickness, using a small and lightweight digital EM system. Journal of Applied Geophysics, 67, 234-241.

[4] Niioka, Tsukasa, and CHO, Kohei, 2010. Sea ice thickness measurement from an ice breaker using a stereo imaging system consisted of a pairs of high definition video cameras. International Archives of the photogrammetry, Remote sensing and spatial information science, XXXVIII, part 8, 1053-1056.

[5] Toyota, T, Nakamura, K, Uto, S, Ohshima, K I, Ebuchi, N. 2009. Retrieval of sea ice thickness distribution in the seasonal ice zone from airborne L-band SAR. International Journal of Remote Sensing, 30(12), 3171-3189.

[6] Worby, A. P., Griffin, P. W., Lytle, V. I., Massom, R. A., 1999. On the use of electromagnetic induction sounding to determine winter and spring sea ice thickness in the Antarctic. Cold Regions Science and Technology, 29, 49-58.

[7] Knuth, M. F., Ackley, S. F., 2006. Summer and early-fall sea-ice concentration in the Ross Sea: comparison of in situ ASPeCt observations and satellite passive microwave estimates. Annual Glaciolgy, 44, 303-309.

[8] Worby, A. P., Comiso, J. C., 2004. Studies of the Antarctic sea ice edge and ice extent from satellite and ship observations. Remote sensing of environment, 92:98-111.

[9] Heil, P., Fowler, C. W., Maslanik, J. A., Emery, W. J., and Allison, I., 2001. A comparison of east Antarctic sea-ice motion derived using drifting buoys and remote sensing, Annals of Glaciology, 33(1):139-144.

[10] Vesecky, J.F., Samadani, R., Smith, M.P., Daida, J.M., and Bracewell, R.N., 1988. Observation of sea -ice dynamics using synthetic aperture radar automated analysis, IEEE Transaction on Geoscience and remote Sensing, 26(1):38-48.

[11] Muramoto, K, Matsuura, K, Endoh, T., 1993. Measuring sea-ice concentration and floe-size distribution by image processing. Annals of Glaciology, 1(18), 33-38.

[12] Hall, R J, Hughes, N, Wadhams, P., 2002. A systematic method of obtaining ice concentration measurements from ship-based observations. Cold Regions Science and Technology, 34(2), 97-102.

[13] Weissling, B., Ackley, S., Wagner, P., and Xie, H., 2009. EISCAM-Digital image acquisition and processing for sea ice parameters from ships. Cold Regions Science and Technology, 57, 49-60.

[14] Lu, P. and Li, Z., 2010. A method of obtaining ice concentration and floe size from shipboard oblique sea ice images. IEEE Transactions on Geosciences and Remote Sensing, 48(7): 2771-2780.

[15] Otsu, N. A., 1979. A threshold selection method from gray-level histograms. IEEE Transactions on systems, man, and cybernetics, SMC-9(1): 62-66.

[16] Harris, C. and Stephens, M. A., 1988. A combined corner and edge detector. Proceedings of the 4th Alvey Vision Conference, Manchester, UK, 147-151.

[17] Vlassis, N., Likas, A., 2002. A greedy EM algorithm for Gaussian mixture learning. Neural Processing Letters, 15:77-87.

[18] Cordelia, S, Roger, M, Christian, B., 2000. Evaluation of interest point detectors. International Journal of Computer Vision. 37(2), 151-172.

Huihui Li, Beijing Branch, CNOOC Information Technology CO, Ltd, Beijing, China.

Jiwen Song, Beijing Branch, CNOOC Information Technology CO, Ltd, Beijing, China.